ISSN 0021-3640, JETP Letters, 2016, Vol. 104, No. 10, pp. 730–741. © Pleiades Publishing, Inc., 2016.
Original Russian Text © V.V. Val'kov, D.M. Dzebisashvili, A.F. Barabanov, 2016, published in Pis'ma v Zhurnal Eksperimental'noi i Teoreticheskoi Fiziki, 2016, Vol. 104, No. 10, pp. 745–757.

SCIENTIFIC SUMMARIES

Spin-Polaron Nature of Fermion Quasiparticles and Their *d*-Wave Pairing in Cuprate Superconductors

V. V. Val'kov[a], *, D. M. Dzebisashvili[a], and A. F. Barabanov[b]

[a] *Kirensky Institute of Physics, Siberian Branch, Russian Academy of Sciences, Akademgorodok, Krasnoyarsk, 660036 Russia*

[b] *Institute for High Pressure Physics, Russian Academy of Sciences, Troitsk, Moscow, 108840 Russia*

* *e-mail: vvv@iph.krasn.ru*

Received October 11, 2016

In the framework of the spin-fermion model, to which the Emery model is reduced in the limit of strong electron correlations, it is shown that the fermion quasiparticles in cuprate high-T_c superconductors (HTSCs) arise under a strong effect of exchange coupling between oxygen holes and spins of copper ions. This underlies the spin-polaron nature of fermion quasiparticles in cuprate HTSCs. The Cooper instability with respect to the *d*-wave symmetry of the order parameter is revealed for an ensemble of such quasiparticles. For the normal phase, the spin-polaron concept allows us to reproduce the fine details in the evolution of the Fermi surface with the changes in the doping level x observed in experiment for $La_{2-x}Sr_xCuO_4$. The calculated T–x phase diagram correlates well with the available experimental data for cuprate HTSCs.

DOI: 10.1134/S002136401622015X

1. INTRODUCTION

The studies of high-T_c superconductors (HTSCs) suggest the existence of strong correlations between the charge and spin degrees of freedom existing in these materials. For example, the pseudogap state in underdoped copper oxides [1, 2] and the $d_{x^2-y^2}$-wave symmetry type of the superconducting order parameter [3, 4] are usually attributed to such correlations.

The theoretical concepts concerning the nature of the Cooper instability in HTSCs and, in particular, those invoking the role of spin–charge fluctuations in the whole mechanism of the superconducting pairing have mostly been developed in the framework of the Hubbard model [5–7], as well as using the t–J and t–J^* models [8–11]. Their specific feature is that a single fermion system possesses both charge and spin degrees of freedom.

At the same time, the actual structure of the CuO_2 plane in cuprate HTSCs is characterized by the spatial separation of spins at copper ions and oxygen holes. In addition, the real unit cell includes two oxygen ions. These facts complicate the description of the energy structure of the fermion excitations; moreover, as was recently learned, they significantly affect the contributions of the Coulomb interaction to the superconducting pairing of different symmetries. The actual significance of this statement is related to establishing the correspondence between the symmetry type of the superconducting order parameter observed in experiment and that following from the theory [12]. It is well known that these features determined by the structure of the CuO_2 plane are adequately described by the three-band p–d model [13–15]. The comparison of theoretical results obtained in the framework of such a model with the experimental data suggests an important role of hybridization between *d* states at each copper ion and *p* states of the four nearest-neighbor oxygen ions. Therefore, the holes appearing because of the doping are accompanied by the formation of a strongly coupled spin–fermion state, namely, a Zhang–Rice singlet [16]. Hence, the theory of the normal and superconducting states in cuprates should include this spin–fermion coupling.

The attempts undertaken in this direction were based, for example, on the projection technique used to reduce the dynamics of oxygen holes to the dynamics of fermions in the subspace of the aforementioned singlet states. The goal was to obtain the Hubbard model or the single-band t–J model as an effective model describing the electronic structure of the CuO_2 plane [17].

However, such scenario implies an important drawback coming from the absence of the spin-correlated hoppings in the t–J model, whereas a more accurate analysis leads to such hoppings [18] playing a

significant role in the formation of the spectral characteristics of fermion quasiparticles.

This discrepancy is lifted if we take into account that the true relations between the parameters of the three-band p–d model correspond to the strong correlation limit. Then, the implementation of the operator form of perturbation theory [19] allows constructing the effective Hamiltonian $\mathcal{H}_{\text{eff}}$, for which the Hilbert space involves only the homopolar states of copper ions. In this case, the hybridization effects become transformed to the additional effective interactions. Among them, the strong spin–fermion coupling between the spins of copper ions and those of oxygen holes is the most significant one. The Hamiltonian $\mathcal{H}_{\text{eff}}$ thus obtained corresponds to the spin–fermion model [20–22]. It is important that such model retains both two hole subsystems and the spatial separation between copper ions and the mentioned subsystems of oxygen holes.

In the framework of the spin–fermion model, the spin-polaron scenario for the formation of charge excitations in the normal phase of cuprate HTSCs was developed [23–25]. In these studies, the concept of spin polaron was implemented on the basis of the Zwanzig–Mori projection technique [26, 27]. The key issue of such a theory is that the basis set of operators includes the operator adequately representing the strong spin–charge coupling. Within this approach, the spectrum of spin-polaron hole excitations was calculated and the important role of the direct oxygen–oxygen hole hoppings was revealed [23]. In the framework of the self-consistent Born approximation, the spectral intensity of spin polarons was calculated and the quasiparticle peak was found close to the bottom of the dispersion curve for unrenormalized holes at the point $(\pi/2, \pi/2)$ [24]. In addition, the changes in the spin-polaron band were analyzed including the coupling of a local polaron to an antiferromagnetic spin wave having the wave vector $Q = (\pi, \pi)$ [28].

In this review, we report recent studies of the characteristics of cuprate HTSCs that were based on the spin-polaron concept and supported by the Russian Foundation for Basic Research.

The first set of results deals with the further development of the spin-polaron approach to the analysis of the normal phase. In particular, we have obtained for the first time the explicit expressions describing the energy spectrum of spin-polaron quasiparticles. By the analysis of spectral curves, we demonstrate the spin-polaron genesis of these quasiparticles. We describe the evolution of the Fermi surface in the specific $La_{2-x}Sr_xCuO_4$ compound within a wide range of doping levels x. Here, the only fitting parameter of the theory is the integral for hole tunneling between the nearest oxygen ions.

The second set of results is related to the formulation of the theory of superconductivity for cuprates in the framework of the spin-polaron approach. For the first time, we reveal the Cooper instability with respect to the $d_{x^2-y^2}$-wave order parameter in the ensemble of spin-polaron quasiparticles. It is shown that the exchange interaction between the spins at copper ions plays the role of the coupling constant. The phase diagram obtained correlates well with the experimental data.

2. HAMILTONIAN OF THE SPIN-FERMION MODEL FOR THE CuO_2 PLANE

It is well known that the SU(2)-invariant spin-fermion model evolves from the three-band Emery model in the limit of strongly correlated electrons. This limit occurs when the mixing parameter t_{pd} between the p states of oxygen ions and d states of copper is much smaller than (i) the energy difference $\Delta_{pd} = \varepsilon_p - \varepsilon_d$ between these states and (ii) the energy of the onsite Coulomb repulsion U_d for two holes at a copper ion. The Hamiltonian of the spin-fermion model can be written in the form [20, 21]

$$\hat{\mathcal{H}} = \varepsilon_p \sum_l c_l^+ c_l + t \sum_{l\rho} \varrho(\rho) c_l^+ c_{l+\rho} + \tau \sum_{f\delta\delta'} u_{\delta\delta'} c_{f+\delta}^+ c_{f+\delta'} + \frac{J}{4} \sum_{f\delta\delta'} u_{\delta\delta'} c_{f+\delta}^+ \tilde{S}_f c_{f+\delta'} + \hat{\mathcal{H}}_{\text{exch}}, \quad (1)$$

where

$$\tau = \frac{(t_{pd})^2}{2}\left[\frac{1}{\Delta_{pd}} - \frac{1}{U_d - \Delta_{pd}}\right],$$

$$J = 4(t_{pd})^2\left[\frac{1}{\Delta_{pd}} + \frac{1}{U_d - \Delta_{pd}}\right].$$

The first term in Eq. (1) describes the energy of coupling between a doped hole and an oxygen ion. The energy ε_p is measured from the chemical potential μ. The operator $c_l^+ = (c_{l\uparrow}^+, c_{l\downarrow}^+)$ in the spinor representation corresponds to the creation of a hole at the lth oxygen ion.

The second term in Eq. (1) corresponds to direct hoppings of holes between the nearest oxygen ions connected by vectors ρ. The hopping intensity is determined by the tunneling integral $t\varrho(\rho)$. Its sign is related to the function $\varrho(\rho)$, depending on the orientation of the line connecting the oxygen ions between which the hopping occurs. The vector ρ spans four values $\pm(g_x + g_y)/2$ and $\pm(g_x - g_y)/2$ (where $\{\pm g_x, \pm g_y\}$ are the vectors corresponding to the four nearest neighbors in the copper lattice) and connects the oxygen ion at the lth site to the oxygen ion nearest to it at the $(l + \rho)$th site. For the chosen phases of the oxygen orbitals, $\varrho(\rho = \pm(g_x + g_y)/2) = 1$ and $\varrho(\rho = \pm(g_x - g_y)/2) = -1$.

The third and fourth terms in Eq. (1) come from the second-order processes in terms of the hybridization parameter t_{pd}. The operators arising here describe the hoppings of a hole between oxygen ions directly adjacent to a copper ion. The vectors δ and δ' independently acquire four values $\{\pm g_x/2, \pm g_y/2\}$ and connect the copper ion at the fth site to the four nearest-neighbor oxygen sites located at positions $f + \delta$. In Eq. (1), $u_{\delta\delta'} = \vartheta(\delta)\vartheta(\delta')$, where $\vartheta(\delta)$ takes into account the effect of relations between the phases of the copper and oxygen orbitals on the hybridization processes. For the usually employed orbitals, $\vartheta(\delta = \pm g_x/2) = \vartheta(\delta = \pm g_y/2) = \mp 1$.

The operator $\tilde{S}_f$ in the fourth term in Eq. (1) has the form $\tilde{S}_f = \mathbf{S}_f\boldsymbol{\sigma}$, where $\mathbf{S}_f$ is the spin moment operator at a copper ion located at the fth site and $\boldsymbol{\sigma} = (\sigma^x, \sigma^y, \sigma^z)$ is the vector of the Pauli matrices. Therefore, in contrast to the second and third terms describing the usual hole hoppings, the fourth term in Hamiltonian (1) takes into account the hoppings accompanied by the spin-flip processes. Such hoppings result in the correlated change in the spin projection not only at the hole but also at the copper ion. Such contributions substantially affect the formation of the structure characteristic of the spin-polaron spectrum of elementary excitations.

The last term in Eq. (1) describes the exchange interaction between the spins of copper ions. The magnitude of the exchange coupling between the spins located at the fth and mth sites is determined by the parameter I_{fm}. Further on, we take into account only the interactions between spins located within two coordination spheres

$$\hat{\mathcal{H}}_{\text{exch}} = \frac{I_1}{2}\sum_{fg}\mathbf{S}_f\mathbf{S}_{f+g} + \frac{I_2}{2}\sum_{fd}\mathbf{S}_f\mathbf{S}_{f+d}. \qquad (2)$$

Here, I_1 denotes the exchange integral for the nearest-neighbor spins and I_2 ($d = \pm g_x \pm g_y$) is the exchange integral for the next-nearest-neighbor spins. It is convenient to express the coupling constants in terms of the frustration parameter p and the effective exchange integral I:

$$I_1 = (1-p)I, \quad I_2 = pI, \quad 0 \le p \le 1, \quad I > 0. \qquad (3)$$

The parameter p can be related to the hole density x per copper atom [25].

The subsystem of spins localized at copper ions is considered in the state of quantum spin liquid, which is characterized by spherical symmetry in the spin state [29–31]. This means that the spin correlation functions $C_j = \langle \mathbf{S}_f\mathbf{S}_{f+r_j}\rangle$ satisfy the relations

$$C_j = 3\langle S_f^x S_{f+r_j}^x\rangle = 3\langle S_f^y S_{f+r_j}^y\rangle = 3\langle S_f^z S_{f+r_j}^z\rangle, \qquad (4)$$

where r_j is the radius of the jth coordination sphere. In addition, $\langle S_f^\alpha\rangle = 0$, $(\alpha = x, y, z)$.

To simplify the form of Hamiltonian (1) and, hence, the further calculations, we perform the unitary transformation of the fermion operators $c_l \to e^{-iQl}c_l$, where $Q = (\pi, \pi)$. After this transformation, the factors $\exp\{iQ(l-l')\}$ appear in the terms containing c-operators in Eq. (1). These factors compensate the signs determined by the functions $\varrho(\rho)$ and $u_{\delta\delta'}$; therefore, we can omit the sign functions in (1). After the unitary transformation $c_l \to e^{-iQl}c_l$, the Hamiltonian of the spin–fermion model takes the form

$$\hat{\mathcal{H}} = \varepsilon_p\sum_l c_l^+ c_l - t\sum_{l\rho} c_l^+ c_{l+\rho} + \tau\sum_{f\delta\delta'} c_{f+\delta}^+ c_{f+\delta'} + \frac{J}{4}\sum_{f\delta\delta'} c_{f+\delta}^+ \tilde{S}_f c_{f+\delta'} + \hat{\mathcal{H}}_{\text{exch}}. \qquad (5)$$

To obtain the expressions describing the spectrum and the spectral intensity as functions of the wave vector k for the untransformed Hamiltonian, it is sufficient to perform the shift $k \to k + Q$ at the end of calculations.

Further on, we take the following commonly used parameters: $t_{pd} = 1.3$ eV, $\Delta_{pd} = 3.6$ eV, $U_d = 10.5$ eV, and $I = 0.13$ eV [32–34]. Then, we have $\tau = 0.11$ eV and $J = 2.86$ eV. In this theory, the tunneling integral t is the fitting parameter, which we will choose on the basis of comparison with the experimental data for $La_{2-x}Sr_xCuO_4$ [35].

3. FERMION STATES IN THE LIMIT OF STRONG CORRELATIONS

To prove the spin-polaron nature of fermion quasiparticles arising within the CuO_2 plane at low doping, let us consider a solution of the Schrödinger equation for a single hole using the variational technique. We will take into account that, according to the Mermin–Wagner theorem [36], the undoped 2D subsystem of localized spin moments corresponds to the state $|G\rangle$ without the long-range magnetic order at any temperature as low as is wished. For the antiferromagnetic exchange coupling, this state has the characteristics [37]

$$\mathbf{S}_{\text{tot}}^2|G\rangle = 0|G\rangle, \quad \langle G|S_f^{x,y,z}|G\rangle = 0, \quad \mathbf{S}_{\text{tot}} = \sum_f \mathbf{S}_f. \qquad (6)$$

The assumption concerning the singlet nature of the state exhibited by the 2D system under study at a nonzero temperature is based on the Marshall theorem [38] stating that a set of an arbitrarily large but finite number of spins that are located at the sites of a square

lattice and are antiferromagnetically coupled with each other has a singlet ground state.

Taking into account the symmetry characteristics of the Hamiltonian, we find that, for any irreducible representation of the translation group k, the single-hole state $|\psi_{k\sigma}\rangle$ with the spin projection σ can be written in the form

$$|\psi_{k\sigma}\rangle = \sum_j \alpha_{jk} A^+_{jk\sigma}|G\rangle, \quad (7)$$

where $A^+_{jk\sigma}$ are both the usual creation operators of a hole on the oxygen subsystem and the combinations of the products of the hole creation operators and the operators corresponding to the localized subsystem (see below).

Using the stationarity condition for the energy functional with the additional constraint $\langle\psi_{k\sigma}|\psi_{k\sigma}\rangle = 1$, we employ the Lagrange method and find that the excitation energies $\varepsilon_k = E_k - E_G$ (E_k and E_G are the energies corresponding to the $|\psi_{k\sigma}\rangle$ and $|G\rangle$states, respectively) and factors α_{jk} are determined by the set of linear homogeneous equations

$$\sum_j \left[D_{ij}(k) - \varepsilon_k K_{ij}(k)\right]\alpha_{jk} = 0, \quad (8)$$

where

$$D_{ij}(k) = \langle G|\{[A_{ik\sigma}, \hat{\mathcal{H}}]_-, A^+_{jk\sigma}\}|G\rangle, \quad (9)$$

$$K_{ij}(k) = \langle G|\{A_{ik\sigma}, A^+_{jk\sigma}\}|G\rangle. \quad (10)$$

The numerical calculations demonstrate that the optimum (for attaining the minimum energy with the minimum set of basis operators) description of the single-hole sector is achieved with three families of the operators

$$A_{1(2)f\sigma} \equiv c_{f+\frac{g_{x(y)}}{2},\sigma}, \quad A_{3f\sigma} = \frac{1}{2}\sum_\delta \left(\tilde{S}_f c_{f+\delta}\right)_\sigma, \quad (11)$$

used to construct the operators in the crystal momentum representation

$$A_{jk\sigma} = N^{-1/2}\sum_f e^{-ikf} A_{jf\sigma} \quad (j = 1,2,3). \quad (12)$$

For each k and σ, operators determine three states: $A^+_{jk\sigma}|G\rangle$ ($j = 1,2,3$). It is easy to check the orthogonality of these states taking into account conditions (6): $\langle G|A_{ik\sigma}A^+_{jq\sigma'}|G\rangle = \delta_{ij}\delta_{kq}\delta_{\sigma\sigma'}K_{jj}(k)$.

Calculating matrix elements (9) and (10), we find ($K_{ij} = \delta_{ij}K_{ii}$)

$$K_{11}(k) = K_{22}(k) = 1, \quad K_{33}(k) = \frac{3}{4} + C_1\gamma_1(k), \quad (13)$$

$$D_{1\,1(22)} = \varepsilon_p + 2\tau\left(1 + \cos k_{x(y)}\right),$$

$$D_{12} = D^*_{21} = (\tau - t)\left(1 + e^{ik_x}\right)\left(1 + e^{-ik_y}\right),$$

$$D_{1(2),3} = D^*_{3,1(2)} = \frac{J}{2}K_{33}\left(1 + e^{ik_{x(y)}}\right), \quad (14)$$

$$D_{33} = \left(\varepsilon_p - 2t + 5\tau - J\right)K_{33} + 2(\tau - t)\left(C_1\gamma_{1k} + C_2\gamma_{2k}\right) + \tau\left(C_1\gamma_{1k} + C_3\gamma_{3k}\right) + JC_1(1/4 - \gamma_{1k}) + I_1C_1(\gamma_{1k} - 4) - 4I_2C_2.$$

Here, γ_{jk} ($j = 1,2,3$) are the invariants corresponding to the square lattice: $\gamma_{1k} = (\cos k_x + \cos k_y)/2$, $\gamma_{2k} = \cos k_x \cos k_y$, and $\gamma_{3k} = (\cos 2k_x + \cos 2k_y)/2$.

The spin correlation functions C_1, C_2, and C_3 in Eqs. (13) and (14) are defined in the same way as in Eq. (4) with the only difference that the averaging of spin operators is performed over the $|G\rangle$ states, $C_j = \langle G|\mathbf{S}_f\mathbf{S}_{f+r_j}|G\rangle$, rather than over the thermodynamic ensemble. In Section 4, we discuss in detail the choice of the correlation functions C_j.

The results of numerical calculations presented in Figs. 1 and 2 demonstrate the importance of the interaction between the charge and spin degrees of freedom, as well as the spin-polaron character of the lower branch in the spectrum of single-hole states. In Fig. 1a, we illustrate the energy spectrum of the single-hole states for the values of the crystal momentum located at the main diagonal of the Brillouin zone. This spectrum is obtained with the use of only two operators, $A_{1k\sigma}$ and $A_{2k\sigma}$. In fact, these branches describe the spectrum of holes which do not interact with the subsystem of spin moments of copper ions.

The addition of the third operator, $A_{3k\sigma}$, to the variation procedure results in the important qualitative changes seen in the spectrum of the single-hole states that was obtained with the three-operator basis and is shown in Fig. 1b by solid lines. The main difference is the appearance of the split-off branch with the minimum at a point close to $(\pi/2, \pi/2)$. The lowering in the energy of such single-hole states is related to the term in the Hamiltonian proportional to $\sim J$, which describes both the exchange interaction between the hole and the nearest copper ions and the spin-correlated hoppings. Just the inclusion of the operators explicitly taking into account this strong spin–fermion correlation in the basis ensures a significant energy gain. This is also accompanied by the renormalization of two initial spectral branches.

The physical reason for the formation of spin-polaron states is similar to that giving rise to the spin polaron in the exactly solvable problem concerning a single electron with the flipped spin in the ferromagnetic host material at the antiferromagnetic type of s–d exchange coupling between the electron spin and the localized spin moment [39].

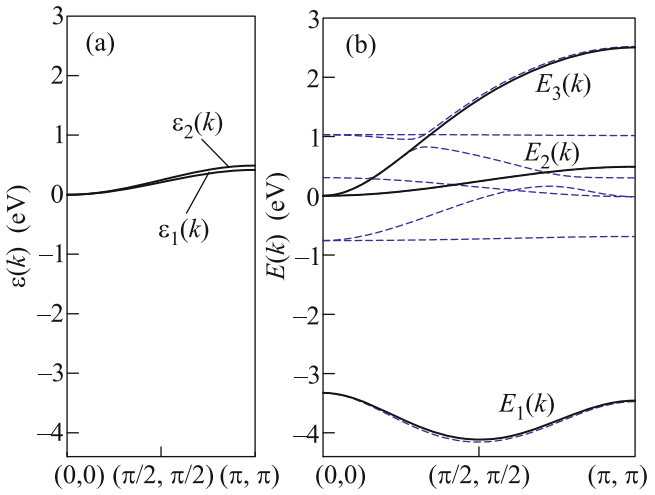

Fig. 1. (Color online) Energies of single-hole states versus the crystal momentum along the main diagonal of the Brillouin zone at the parameters $\tau = 0.11$ eV, $J = 2.86$ eV, $t = 0.1$ eV, and $I = 0.2\tau$. The spin correlation functions are $C_1 = -0.255$, $C_2 = 0.075$, and $C_3 = 0.064$. (a) Energy spectrum $\varepsilon_j(k)$ obtained taking into account two operators $A_{1k\sigma}$ and $A_{2k\sigma}$. (b) Energies of single-hole states $E_j(k)$ calculated using (solid lines) the three-operator basis given by Eq. (11) and (dashed lines) the eight-operator basis specified by Eq. (15). The lower spectral branches coinciding for both bases correspond to spin-polaron states.

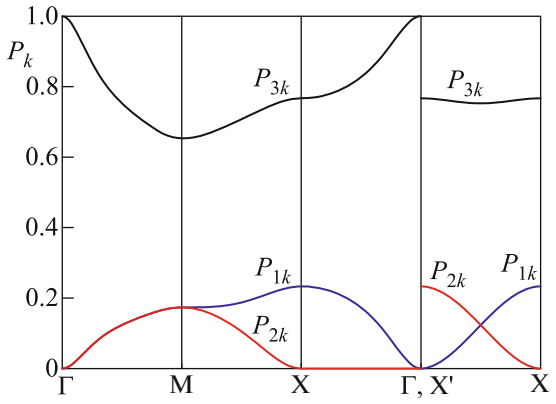

Fig. 2. (Color online) Partial contributions of basis states to the single-hole state, corresponding to the lower branch of the spectrum shown in Fig. 1b. The characteristic parameters of the model used for calculations of these plots are chosen to be the same as those corresponding to the curves in Fig. 1. Here, $\Gamma = (0, 0)$, $M = (\pi, \pi)$, $X = (0, \pi)$, and $X' = (\pi, 0)$.

For the crystal momentum spanning other directions of the Brillouin zone, the qualitative changes in the energy spectrum of single-hole states hold.

It is important to note that the split-off lower spin-polaron band remains with an increase in the number of basis operators. To illustrate this statement, we show in Fig. 1b the results of the variational calculation of the fermion spectrum in the framework of the basis consisting of eight operators

$$\tilde{A}_{jk} = N^{-1/2}\sum_f e^{-ikf}\tilde{A}_{jf} \quad (j = 1,\ldots,8), \tag{15}$$

where

$$\tilde{A}_{1(2)f} = c_{f+\frac{g_{x(y)}}{2}}, \quad \tilde{A}_{3(4)f} = \tilde{S}_f c_{f+\frac{g_{x(y)}}{2}},$$

$$\tilde{A}_{5(6)f} = \tilde{S}_f c_{f-\frac{g_{x(y)}}{2}}, \quad \tilde{A}_{7(8)f} = \mathbf{S}_f\mathbf{S}_{f+g_{x(y)}} c_{f+\frac{g_{x(y)}}{2}}.$$

The first two operators of this basis coincide with the corresponding operators of basis (11). Each of four operators $\tilde{A}_{jk}$ with $j = 3, \ldots, 6$ describes the correlation of a localized spin with a hole located at one of the four nearest-neighbor oxygen ions. The last two operators, $\tilde{A}_{7k}$ and $\tilde{A}_{8k}$, describe the correlation of a hole located at an oxygen ion simultaneously with two spins located at the two nearest copper ions. The calculated eight branches of the fermion spectrum are shown in Fig. 1b by dashed lines. It is important that the dispersion law for the lower branch of the spin-polaron spectrum remains nearly unchanged. Hence, the three-operator basis (11) is sufficient with a high accuracy for the description of the low-energy part in the spectrum of fermion quasiparticles.

In the low-doping limit characteristic of cuprate HTSCs, the chemical potential always lies in the lower spin-polaron band. For this reason, the problem of obtaining an explicit expression for the dispersion law $E_1(k)$ in this band is quite significant. To solve this problem, we use the following equation for finding the dispersion relation:

$$\det_k(\omega) = \left|D(k) - \omega K(k)\right| = 0, \tag{16}$$

whose roots determine the frequencies ω for which the solutions α_{jk} of Eqs. (8) are nontrivial. Representing the determinant in Eq. (16) in the explicit form, we obtain the expression

$$\det_k(\omega) = (\omega - \varepsilon_p)^3 - Q_k(\omega - \varepsilon_p)^2 + B_k(\omega - \varepsilon_p) + R_k = 0, \tag{17}$$

where

$$Q_k = 4\tau(1 + \gamma_{1k}) + \Lambda_k,$$

$$B_k = \left(4\tau\Lambda_k - J^2K_{33}\right)(1 + \gamma_{1k}) + 4t(2\tau - t)\chi_k,$$

$$R_k = 4t\chi_k\left[J^2K_{33}/2 - \Lambda_k(2\tau - t)\right],$$

$$\Lambda_k = D_{33}K_{33} - \varepsilon_p, \quad \chi_k = 1 + 2\gamma_{1k} + \gamma_{2k}. \tag{18}$$

For the used set of parameters, it is easy to obtain approximate solutions of the dispersion equation (17) describing with a high accuracy the spectral functions $E_j(k)$ $(j = 1, 2, 3)$ for the single-hole states. Then, the

spin-polaron spectrum is determined by the expression

$$E_1(k) = \varepsilon_p + x_k, \quad x_k = \frac{Q_k}{2} - \sqrt{\frac{Q_k^2}{4} - B_k - \frac{R_k}{x_{k0}}}, \quad (19)$$

where $x_{k0} = Q_k/2 - \sqrt{Q_k^2/4 - B_k}$. For the two upper branches $E_2(k)$ and $E_3(k)$ shown in Fig. 1b, we obtain

$$E_{2}_{3}(k) = \varepsilon_p + (Q_k - x_k)/2 \mp \sqrt{(Q_k - x_k)^2/4 + R_k/x_k}. \quad (20)$$

Let us discuss the structure of the single-hole state corresponding to the lower spectral branch $E_1(k)$ in Fig. 1b. The spectral weights P_{1k} and P_{2k} of the bare hole states $A^+_{1k\sigma}|G\rangle$ and $A^+_{2k\sigma}|G\rangle$ are $P_{1k} = |\alpha_{1k}|^2$ and $P_{2k} = |\alpha_{2k}|^2$. The spectral weight of the spin-polaron basis state is $P_{3k} = K_{33}|\alpha_{3k}|^2$.

In Fig. 2, we show the introduced partial contributions for crystal momenta lying at four directions of the Brillouin zone. It is seen that P_{3k} (upper curves) is several times larger than P_{1k} and P_{2k}. This verifies the spin-polaron nature of the single-hole state corresponding to the lower split-off spectral branch.

4. EVOLUTION WITH THE DOPING OF THE FERMI SURFACE IN LSCO

In the preceding section, the spectrum of fermion quasiparticles was calculated by a variational method taking into account the strong coupling between the subsystem of localized spins at copper ions and the spin of an oxygen hole. In fact, we considered only one hole. In the case of a finite number of holes, it is convenient to calculate the spectrum of fermion excitations using the Zwanzig–Mori projection technique [26, 27]. In addition, this technique in combination with the formalism of retarded Green's functions makes it possible to calculate the necessary thermal averages and, as is shown below, to describe the Cooper instability in the ensemble of spin polarons.

In the framework of the projection technique, we choose the minimal basis consisting of n operators A_{jf} ($j = 1,\ldots,n$), which is assumed to be sufficient for an adequate description of quasiparticle excitations in the system. Then, we introduce the two-time retarded Green's functions ($i, j = 1,\ldots,n$)

$$G_{ij}(k,t) = \langle\langle A_{ik}(t)|A^+_{jk}(0)\rangle\rangle = -i\theta(t)\langle[A_{ik}(t), A^+_{jk}(0)]\rangle,$$

where the operator A_{jk} is related to the operator A_{jf} through Eq. (12). The equations of motion for the Fourier transforms of the introduced Green's functions have the form

$$\omega\langle\langle A_{ik}|A^+_{jk}\rangle\rangle = K_{ij}(k) + \langle\langle[A_{ik}, \hat{\mathcal{H}}]|A^+_{jk}\rangle\rangle_\omega, \quad (21)$$

where

$$K_{ij}(k) = \langle\{A_{ik}, A^+_{jk}\}\rangle. \quad (22)$$

Projecting the commutation relation $[A_{ik}, \hat{\mathcal{H}}]$ onto the chosen operator basis, we obtain

$$[A_{ik}, \hat{\mathcal{H}}] = \sum_l L_{i,l}(k)A_{lk}, \quad (23)$$

where $L(k) = D(k)K(k)^{-1}$ and

$$D_{ij}(k) = \langle\{[A_{ik}, \hat{\mathcal{H}}], A^+_{jk}\}\rangle. \quad (24)$$

In Eqs. (22) and (24), the angular brackets denote the thermal averaging over the Gibbs ensemble, whereas the averaging of similar matrices in Eqs. (9) and (10) is performed over the ground state $|G\rangle$ of the system. However, the matrix elements of $D(k)$ and $K(k)$ calculated in the low-density limit coincide for both kinds of definition and are given by Eqs. (13) and (14). Further on, we assume that the matrix elements of $D(k)$ and $K(k)$ are defined according to Eqs. (22) and (24).

Substituting (23) into equations of motion (21), we obtain the closed set of equations for the Green's functions. In the matrix form, this system reads

$$\left(\omega\cdot\hat{I} - D(k)K(k)^{-1}\right)G(k,\omega) = K(k), \quad (25)$$

where $\hat{I}$ is the identity matrix.

The quasiparticle spectrum is determined by the poles of the Green's function $G(k)$ and can be calculated using the dispersion equation

$$\det\left|\omega\cdot K(k) - D(k)\right| = 0. \quad (26)$$

In particular, if we choose operators (11) as the basis operators, Eq. (26) coincides with Eq. (17).

In this section, using the projection technique, we demonstrate the efficiency of the spin-polaron approach by applying it to the angle-resolved photoemission spectroscopy (ARPES) data reported in [35]. In that work, the doping-induced transformation of the Fermi surface in $La_{2-x}Sr_xCuO_4$ (LSCO) was analyzed in detail in the doping range from $x = 0.03$, at which LSCO is an underdoped insulator, to $x = 0.3$, where LSCO undergoes a transition to the state of normal metal. To characterize the Fermi surface, the authors of [35] introduced the Fermi momentum k_F equal to the distance from the $\Gamma = (0,0)$ point in the Brillouin zone to the point where the Fermi surface intersects with the nodal line. The authors of [35] determined k_F as a function of x and demonstrated the transformation of the Fermi surface topology from the electron to hole type at a threshold value of the doping level.

Here, we assume for simplicity that the Coulomb repulsion is $U_d = \infty$. Under this condition, in the Hamiltonian of spin-fermion model (5), we have

$\tau = 0.23$ eV and $J = 1.88$ eV. We choose three operators (11) as the basis operators. The Green's functions determined from Eq. (25) can be represented in the form

$$G_{ij}(k,\omega) = \sum_{n=1}^{3} \frac{z^{n}_{(i,j)}(k)}{\omega - E_n(k)}, \quad i,j = 1,2,3. \qquad (27)$$

As was mentioned above, for cuprate HTSCs, only the lower polaron band with the dispersion law $E_{n=1}(k)$ shown in Fig. 1b comes into play. Two other bands with $n = 2$ and 3 are separated from $E_1(k)$ by a wide band gap.

An important feature of the used approach is that the correlation functions C_1, C_2, and C_3 (determining the matrix elements K_{ij} and D_{ij} according to Eqs. (13) and (14)), as well as the gap $\Delta_Q(p)$ in the spectrum of magnetic excitations near the Q point of the Brillouin zone, are determined simultaneously in the framework of the spherically symmetric self-consistent method developed for a frustrated antiferromagnet [29–31, 37]. Here, Δ_Q is a linear function of the inverse correlation length ξ^{-1}. On the other hand, according to the neutron scattering and nuclear magnetic resonance data (see, e.g., [40, 41]), ξ^{-1} is determined by the doping level x. In LSCO, it increases by several times with x ranging from 0.03 to 0.3. According to this, the values of frustrations specified by us (see table) correspond to the case where the spin gap increases by a factor of 2.5 at the growth of the frustration parameter from $p = 0.15$ to $p = 0.3$.

In the table, we present the spin correlation functions calculated by such a technique for five values of the frustration parameter p, which we relate to five values of the doping level x.

Doping levels x and the corresponding frustration parameters p and the spin correlation functions

x	p	C_1	C_2	C_3
0.03	0.15	−0.287	0.124	0.0950
0.07	0.21	−0.255	0.075	0.0640
0.15	0.25	−0.231	0.036	0.0510
0.22	0.275	−0.214	0.009	0.0450
0.30	0.30	−0.194	−0.0222	0.0457

For LSCO, the Fermi energy can be determined by equating the number of bare holes n_h to the doping level x. The number n_h at small values of x is equal to the spectral density $n_{h,\sigma}(k) = z^{1}_{(1,1)}(k) + z^{1}_{(2,2)}(k)$ integrated over the Brillouin zone and summed over σ.

In Fig. 3, we illustrate the distribution of the spectral density over the Brillouin zone. At the Γ point, we have $n_{h,\sigma}(k) = 0$, but the spectral weight grows steeply with the shift from this point and saturates at approaching the antinodal X–X line.

In Fig. 4, to illustrate the formation of a flat-band region near X points in the k space, we highlight the lower spin-polaron band by $E_1(k) = \text{const}$ contours calculated at $x = 0.15$. The existence of the flat band in this region was reported in numerous studies [42–48]; in particular, such a band was revealed in [35] at $x \le 0.15$. The data presented in Fig. 4 allow estimating the effective mass for polaron quasiparticles,

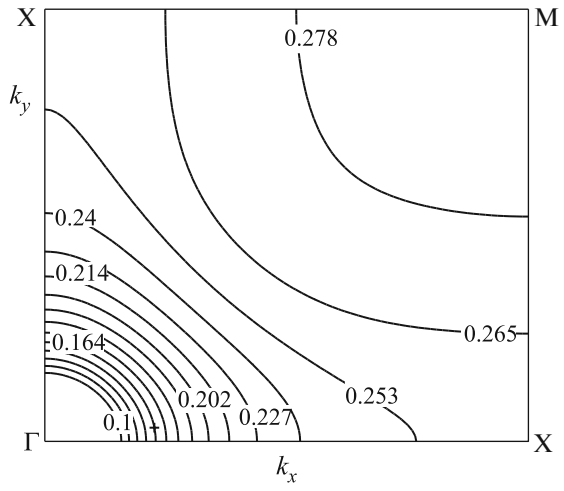

Fig. 3. Contours of the spectral density $n_{h,\sigma}(k)$ corresponding to bare holes in the lower polaron band on the first quarter of the k space at the doping level $x = 0.15$. The numbers indicate the values of $n_{h,\sigma}(k)$.

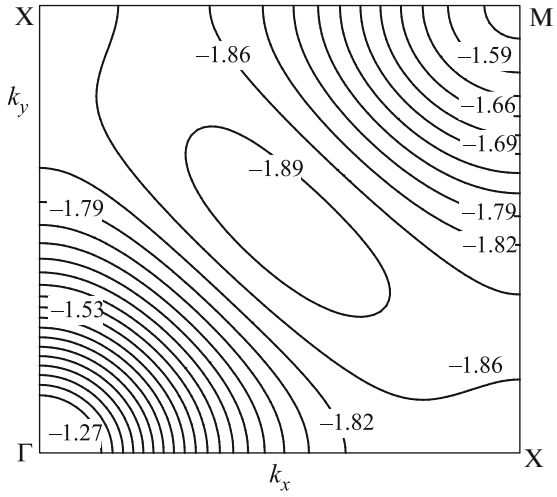

Fig. 4. Contours of the energy $E_1(k) = \text{const}$ in the lower polaron band within the first quarter of the k space at the doping level $x = 0.15$. The numbers indicate the values of $E_1(k)$ in electronvolts.

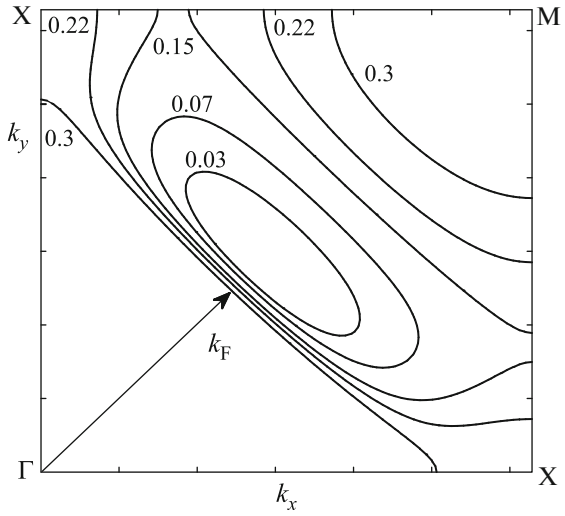

Fig. 5. Fermi surfaces in the first quadrant of the Brillouin zone for five doping levels x indicated near the corresponding Fermi contours.

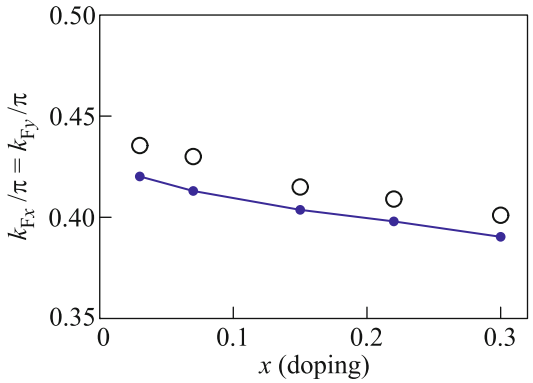

Fig. 6. (Color online) Fermi momentum k_F versus the doping level x. The solid curve connects the values of k_F calculated in the framework of the spin-polaron approach. Open circles denote experimental values of k_F taken from [35].

which, as we can see, is strongly anisotropic. For the nodal ($\Gamma - M$) direction, the calculations give the effective mass $m_{\Gamma-M} = 1.25m_e$, where m_e is the free electron mass, whereas in the antinodal ($X - X$) direction, we have $m_{X-X} = 9.4m_e$.

The $n_{h,\sigma}(k) = \text{const}$ and $E_1(k) = \text{const}$ contours shown in Figs. 3 and 4 are calculated with the value $t = 0.094$ eV of the hopping integral for the direct oxygen–oxygen hoppings. This single fitting parameter is chosen to fit the Fermi surface topology to the ARPES experimental data [35]. We should emphasize that the same t value is used to describe the Fermi surface at all five doping levels x listed in the table.

The Fermi surface calculated simultaneously with the spin correlation at the five aforementioned doping levels x are shown in Fig. 5. The Fermi surface topology changes from the electron to hole type with the increase in x as in the experiment.

The calculated doping dependence of k_F is presented in Fig. 6 in comparison with that measured in [35]. We can see that the weak dependence of k_F on x is well reproduced in the framework of the suggested spin-polaron theory: the maximum disagreement between the experimental and calculated values of k_F does not exceed 4%.

5. SELF-CONSISTENT EQUATIONS FOR THE SUPERCONDUCTING PHASE

The theory describing the superconducting state in the system of oxygen holes strongly coupled to the subsystem of localized spin moments of copper ions in the framework of the spin-polaron approach was formulated for the first time in [49]. For this purpose, it was required to extend the basis operator set so that anomalous averages could be introduced.

Taking into account the results discussed in the previous sections, we can easily see that, to obtain the self-consistent equations for the anomalous averages, three operators $A_{1k\sigma}$, $A_{2k\sigma}$, and $A_{3k\sigma}$ given by Eq. (12) should be supplemented by the three operators

$$A_{4k\sigma} = A^+_{1,-k,\bar{\sigma}}, \quad A_{5k\sigma} = A^+_{2,-k,\bar{\sigma}}, \quad A_{6k\sigma} = A^+_{3,-k,\bar{\sigma}}. \quad (28)$$

With the basis consisting of six operators specified by Eqs. (12) and (28) used in the framework of the projection technique, the set of equations of motion for Green's functions (25) and dispersion equation (26) are now of the sixth order ($n = 6$).

In contrast to the previous section, we will not use here the simplifying condition $U_d = \infty$ and will perform our analysis at $U_d = 10.5$ eV [32]. It is clear that the matrix elements $K_{ij}(k)$ and $D_{ij}(k)$ with subscripts $i, j = 1,\ldots,3$ coincide with those calculated before (see Eqs. (13) and (14)). The matrix $K(k)$ is still diagonal and its diagonal elements obey the condition $K_{j+3,j+3}(k) = K_{jj}(k)$ ($j = 1,\ldots,3$). It is convenient to describe the matrix $D(k)$ in the block representation. The left upper 3×3 block is constructed including only normal averages $D_{ij}(k)$ ($i, j = 1,2,3$). The right lower block is formed by $D_{ij}(k)$ with $i, j = 4,5,6$. Here, we have $D_{i+3,j+3}(k) = -D_{ij}(k)$ for all $i, j = 1,2,3$.

The matrix elements of the right upper block in $D(k)$ are due to anomalous pairings. In the case under study, this block included only one nonzero matrix element $D_{36}(k)$. Since the matrix is Hermitian, the lower left block in $D(k)$ also has only one nonzero matrix element $D_{63}(k)$, coinciding with $D_{36}(k)$.

As a result, we can write the dispersion equation (26) for the superconducting phase in the form

$$\det_k(\omega)\det_k(-\omega) + \varphi_k(\omega)\varphi_k(-\omega)\left|\frac{D_{36}(k)}{K_{33}(k)}\right|^2 = 0, \quad (29)$$

where

$$\varphi_k(\omega) = (\omega + \varepsilon_p)^2 + 4\tau(1+\gamma_{1k})(\omega+\varepsilon_p) + 4t(2\tau - t)\chi(k). \quad (30)$$

In the normal phase, $D_{36}(k) = 0$ and Eq. (29) transforms to Eq. (17).

The anomalous average $D_{36}(k)$ is expressed in terms of the sum of a large number of terms, which can give the solutions of the integral self-consistency equation corresponding to the different symmetry types of the superconducting order parameter. In particular, the terms proportional to the parameter J lead to the s-wave pairing. In view of the available experimental data, we consider only the d-wave superconducting order parameter. In this case, we can use a reduced expression for $D_{36}(k)$

$$D_{36}(k) = I_1\sum_{\delta} e^{ik2\delta}\left[-\langle A^+_{6f\sigma}A_{3,f+2\delta,\sigma}\rangle + \frac{C_1}{4}\sum_{\delta'\delta_1}\langle c_{f+2\delta+\delta_1,\bar{\sigma}}c_{f+\delta',\sigma}\rangle\right]. \quad (31)$$

To derive Eq. (31), we used the following relation for the averages of the operator products, which are not reduced to the basis operators:

$$\left\langle\left(\tilde{S}_f c_l\right)_{\bar{\sigma}}\left(\tilde{S}_g c_{l'}\right)_{\sigma}\right\rangle = 2\left\langle\left(\mathbf{S}_f\mathbf{S}_g\right)c_{l\sigma}c_{l'\bar{\sigma}}\right\rangle - \left\langle\left(\tilde{S}_f c_{l'}\right)_{\bar{\sigma}}\left(\tilde{S}_g c_l\right)_{\sigma}\right\rangle, \quad (32)$$

which is valid for the SU(2)-invariant phase and allows us to express this average in terms of the averages involving the basis operators. Only with the use of this expression does Eq. (31) include the anomalous average $\langle A^+_{6f\sigma}A_{3,f+2\delta,\sigma}\rangle$, which plays, according to the numerical calculations, a crucial role in the formation of the d-wave superconductivity in the ensemble of spin-polaron quasiparticles. For the thermal averages containing the scalar product of spin operators, we employed the decoupling procedure. This gives rise to the magnetic correlation function C_1 appearing in the second term of the right-hand side of Eq. (31).

According to Eq. (31), $D_{36}(k)$ can be written as

$$D_{36}(k) = \Delta_0(\cos k_x - \cos k_y). \quad (33)$$

The amplitude Δ_0 of the superconducting order parameter can be found from the equation

$$1 = \frac{I_1}{N}\sum_k \frac{(\cos k_x - \cos k_y)^2 \tanh\left(\frac{E_k}{2T}\right)}{2E_k\left(E_k^2 - E_2^2(k)\right)\left(E_k^2 - E_3^2(k)\right)} \times\left[\varphi_k(E_k)\varphi_k(-E_k) - C_1J^2\Psi_k(E_k)\Psi_k(-E_k)\right], \quad (34)$$

where

$$\Psi_k(\omega) = (\omega - \varepsilon_p)(1+\gamma_{1k}) - 2t\chi_k, \quad (35)$$

and the spectrum of fermion excitations in the superconducting phase E_k takes the form

$$E_k = \sqrt{E_1^2(k) + b_k^2 D_{36}^2(k)}. \quad (36)$$

Here,

$$b_k^2 = \frac{1}{K_{33}^2}\cdot\frac{\varphi_k(E_1(k))\varphi_k(-E_1(k))}{\left(E_1^2(k) - E_2^2(k)\right)\left(E_1^2(k) - E_3^2(k)\right)}. \quad (37)$$

The self-consistent calculations demonstrate that b_k^2 is close to unity within nearly the whole Brillouin zone.

It follows from Eq. (36) that the spectrum of fermion excitations in the superconducting phase is based on the spin-polaron states. According to this, we can argue that the Cooper instability under study corresponds to the instability of just the spin-polaron ensemble.

According to the spectral theorem, the equation for determining the chemical potential μ in the superconducting phase can be written in the form

$$\frac{x}{4} = \frac{1}{N}\times\sum_k \frac{\mathcal{J}_k(E_k)f(E_k/T) - \mathcal{J}_k(-E_k)f(-E_k/T)}{2E_k\left(E_k^2 - E_2^2(k)\right)\left(E_k^2 - E_3^2(k)\right)}, \quad (38)$$

where

$$\mathcal{J}_k(\omega) = \left(-\omega + \varepsilon_p + 2\tau(1+\gamma_{1k})\right)\varphi_k(\omega)\frac{|D_{36}(k)|^2}{K_{33}(k)} - \Big[\left(\omega - \varepsilon_p - 2\tau(1+\gamma_{1k})\right)\left(\omega - D_{33}(k)/K_{33}(k)\right) - (J^2/2)K_{33}(k)(1+\gamma_{1k})\Big]\det_k(-\omega) \quad (39)$$

and $f(z) = 1/(\exp(z)+1)$ is the Fermi–Dirac function.

6. EFFECT OF DOPING ON THE COOPER INSTABILITY OF THE SPIN-POLARON ENSEMBLE

The doping dependence of the critical temperature for the transition to the superconducting phase with the d-wave order parameter is calculated by solving Eq. (34) along with Eq. (38) determining the chemical potential.

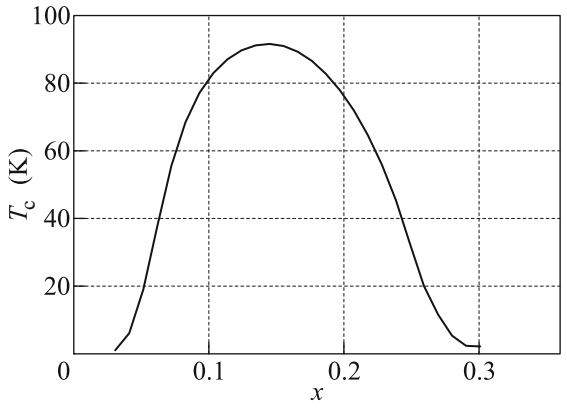

Fig. 7. Temperature of the transition to the superconducting phase with the *d*-wave symmetry of the superconducting order parameter. The characteristic parameters of the model used for the calculation of this plot are chosen to be the same as those corresponding to the dispersion curves shown in Fig. 1.

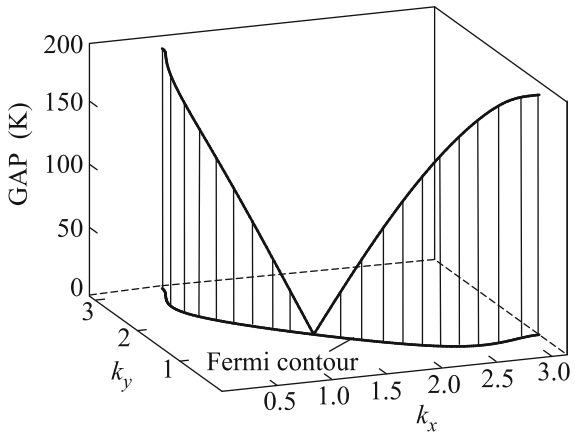

Fig. 8. Superconducting gap versus the crystal momentum in the Fermi contour. The Fermi contour is shown by the solid line in the horizontal plane. The calculation is performed at $x = 0.125$ and $T = 0$. The other parameters of the model are chosen to be the same as those used in Fig. 1.

The numerical calculations were performed taking into account that K_{ij} and D_{ij} depend on the spin correlation functions C_j given by Eq. (4) for the first three coordination spheres $j = 1, 2, 3$. These correlation functions are determined self-consistently using the technique described in Section 4. The change in the density of holes x is taken into account by the modification of spin correlation functions C_j, by the displacement of the chemical potential μ, and by the renormalization of parameter $I_1 = I(1 - p)$ playing the role of a coupling constant (see Eq. (34)).

The exchange integral I is determined using the formula $T_N = \pi I/(\log(I/\sqrt{KK'}) + 3.5)$ obtained in [50], where the bilayer system $YBa_2Cu_3O_{6+x}$ was studied. Here, K and K' are the exchange integrals for the ions in the nearest planes and in the planes in the adjacent unit cells, respectively. Taking into account a weak dependence of I on the constants K and K', which are of the order of 10^{-3}–10^{-2} eV, we obtain $I \approx 0.1$ eV (or $I = 0.2\tau$) for the Néel temperature $T_N = 400$ K [51], which is in good agreement with the available experimental data. The doping dependence of the critical temperature calculated for this value of I is shown in Fig. 7. We can see that the famous superconducting dome is well reproduced in both the value of T_c and the doping range x.

The phase diagram represented in Fig. 7 was obtained with the tunneling integral $t = 0.1$ eV for the nearest oxygen ions, i.e., the same as that used in Section 4 to describe the evolution of the Fermi surface. In Section 4, the t value was chosen by fitting the experimental and calculated Fermi surface and $k_F(x)$ functions. Here, according to the self-consistent calculations, the integral t significantly affects the position of the lower boundary x_c of the superconducting dome, corresponding to the low doping levels. It turns out that the measured value $x_c \approx 0.05$ is achieved just for $t = 0.1$ eV. Thus, the comparison of the experimental data with the calculations in the framework of the spin-polaron approach for both the normal and superconducting phases leads to the same value $t = 0.1$ eV. This value significantly differs from often used values $t = 0.4$–0.6 eV [32–34, 52].

In Fig. 8 we demonstrate the variation of the band gap appearing in the spectrum of elementary exci-

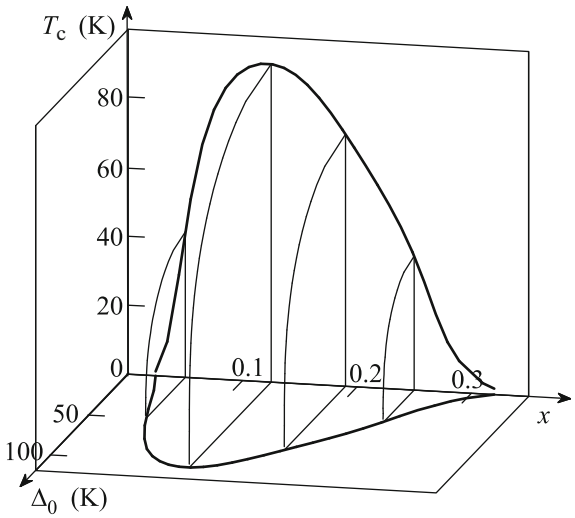

Fig. 9. Doping dependences of the amplitude of the superconducting order parameter and the superconducting transition temperature. The characteristic parameters of the model used for calculations of these plots are chosen to be the same as those corresponding to the curves in Fig. 1.

tations for spin-polaron quasiparticles at the Fermi contour in the superconducting phase. We can see that the dependence of the band gap on the crystal momentum in the first Brillouin zone is characteristic of the *d*-wave symmetry.

In Fig. 9, to find the relation between the order parameter $|D_{36}(k)|$ and critical temperature T_c, we draw their doping dependence. According to this figure, the amplitude of the order parameter vanishes at T_c through a second order phase transition.

7. CONCLUSIONS

The main results of the reviewed studies supported by the Russian Foundation for Basic Research (project no. 13-02-00523) are as follows.

(i) In the framework of the spin-fermion model including the strong coupling between the spin and charge degrees of freedom and the actual lattice structure in the CuO_2 plane with two oxygen ions per unit cell, it has been shown that spin-polaron quasiparticles determine the low-temperature features in the characteristics of cuprate superconductors. For the spin-polaron concept, the crucial role is played by the basis operator characterizing a strong correlation between the subsystem of localized spin moments at copper ions and the subsystem of holes moving via oxygen ions.

(ii) It has been shown that the energy band corresponding to the spin-polaron states is located much lower (by about 3 eV) than the decoupled fermion states. This determines the stability of spin polarons.

(iii) The self-consistent calculations have demonstrated that fine details of the evolution of the Fermi surface in $La_{2-x}Sr_xCuO_4$, which is observed in the ARPES experiments at doping, are well reproduced within the developed spin-polaron concept primarily because of the inclusion of:

(a) the spin-correlated hoppings in the effective Hamiltonian;

(b) the doping-induced changes in the inverse correlation length ξ^{-1};

(c) the k dependence and the small values of the residue function for "bare" holes $n_{h,\sigma}(k)$ in the lower polaron band when determining the Fermi surface. The treatment of the spin subsystem in the framework of the spherically symmetric theory is also important [29–31].

(iv) In the framework of the spin–fermion model, it has been shown for the first time that the ensemble of spin-polaron quasiparticles undergoes a cooling-induced transition to the superconducting state with the *d*-wave superconducting order parameter. Here, the mechanism underlying the Cooper pairing is related to the exchange interaction, which as a result of the strong spin–charge coupling transforms to the effective attraction between spin polarons.

(v) We have obtained simple explicit expressions both for the spin-polaron spectrum in the normal phase and for the spectrum of fermion excitations in the superconducting phase.

(vi) The comparison of the experimental data and the self-consistent numerical calculations both for the normal and for the superconducting phase has shown that the tunneling integral t between the nearest oxygen ions differs from the often-used values and is equal to 0.1 eV. Just at this value of t, the $T-x$ phase diagram obtained in the framework of the spin-polaron concept and the dependence of k_F on the doping level x correlate well with the experimental data for copper oxides.

This work was supported by the Russian Foundation for Basic Research (project nos. 13-02-00523, 16-42-240435, and 16-02-00304) and by the Siberian Branch, Russian Academy of Sciences (project no. 0358-2015-0005, Complex Program II.2P).

REFERENCES

1. M. V. Sadovskii, Phys. Usp. **44**, 515 (2001).
2. E. Z. Kuchinskii and M. V. Sadovskii, JETP Lett. **88**, 192 (2008).
3. Y. A. Izyumov, Phys. Usp. **40**, 445 (1997).
4. N. Plakida, *High-Temperature Cuprate Supercoductors Experiment, Theory, and Applications* (Springer, Berlin, 2010).
5. R. Zaitsev, J. Exp. Theor. Phys. **98**, 780 (2004).
6. N. Plakida, L. Anton, S. Adam, and Gh. Adam, J. Exp. Theor. Phys. **97**, 331 (2003).
7. A. A. Vladimirov, D. Ihle, and N. M. Plakida, Theor. Math. Phys. **152**, 1331 (2007).
8. M. Y. Kagan and T. M. Rice, J. Phys.: Condens. Matter **6**, 3771 (1994).
9. V. V. Val'kov, T. A. Val'kova, D. M. Dzebisashvili, and S. G. Ovchinnikov, JETP Lett. **75**, 378 (2002).
10. V. Val'kov and D. Dzebisashvili, J. Exp. Theor. Phys. **100**, 608 (2005).
11. S. Ovchinnikov, M. M. Korshunov, and E. I. Shneyder, J. Exp. Theor. Phys. **109**, 775 (2009).
12. V. V. Val'kov, D. M. Dzebisashvili, M. M. Korovushkin, and A. F. Barabanov, JETP Lett. **103**, 385 (2016).
13. V. J. Emery, Phys. Rev. Lett. **58**, 2794 (1987).
14. C. M. Varma, S. Schmitt-Rink, and E. Abrahams, Solid State Commun. **62**, 681 (1987).
15. J. E. Hirsch, Phys. Rev. Lett. **59**, 228 (1987).
16. F. C. Zhang and T. M. Rice, Phys. Rev. B **37**, 3759 (1988).
17. P. W. Anderson, Science **235**, 1196 (1987).
18. A. Ramsak and P. Prelovsek, Phys. Rev. B **40**, 2239 (1989).
19. N. N. Bogoliubov, *Lectures on Quantum Statistics* (Naukova Dumka, Kiev, 1949; Gordon and Breach, New York, 1967, 1970).

20. A. Barabanov, L. Maksimov, and G. Uimin, JETP Lett. **47**, 622 (1988).
21. J. Zaanen and A. M. Oles, Phys. Rev. B **37**, 9423 (1988).
22. P. Prelovsek, Phys. Lett. A **126**, 287 (1988).
23. A. Barabanov, V. Berezovskii, E. Zhasinas, and L. A. Maksimov, J. Exp. Theor. Phys. **83**, 819 (1996).
24. R. O. Kuzian, R. Hayn, A. F. Barabanov, and L. A. Maksimov, Phys. Rev. B **58**, 6194 (1998).
25. A. Barabanov, R. Hayn, A. Kovalev, O. V. Urazaev, and A. M. Belemuk, J. Exp. Theor. Phys. **92**, 677 (2001).
26. R. Zwanzig, Phys. Rev. **124**, 983 (1961).
27. H. Mori, Prog. Theor. Phys. **33**, 423 (1965).
28. A. Barabanov, L. Maksimov, E. Zhasinas, and O. V. Urazaev, JETP Lett. **66**, 173 (1997).
29. J. Kondo and K. Yamaji, Prog. Theor. Phys. **47**, 807 (1972).
30. H. Shimahara and S. Takada, J. Phys. Soc. Jpn. **60**, 2394 (1991).
31. A. Barabanov and V. Berezovskii, J. Exp. Theor. Phys. **79**, 627 (1994).
32. M. Ogata and H. Fukuyama, Rep. Prog. Phys. **71**, 036501 (2008).
33. B. Lau, M. Berciu, and G. A. Sawatzky, Phys. Rev. Lett. **106**, 036401 (2011).
34. O. A. Starykh, O. F. de Alcantara Bonfim, and G. F. Reiter, Phys. Rev. B **52**, 12534 (1995).
35. T. Yoshida, X. J. Zhou, D. H. Lu, S. Komiya, Y. Ando, H. Eisaki, T. Kakeshita, S. Uchida, Z. Hussain, Z.-X. Shen, and A. Fujimori, J. Phys.: Condens. Matter **19**, 125209 (2007).
36. N. D. Mermin and H. Wagner, Phys. Rev. Lett. **17**, 1133 (1966).
37. A. F. Barabanov, A. V. Mikheenkov, and A. V. Shvartsberg, Theor. Math. Phys. **168**, 1192 (2011).
38. W. Marshall, Proc. R. Soc. London A **232**, 48 (1955).
39. Y. A. Izyumov and M. Medvedev, Sov. Phys. JETP **32**, 302 (1971).
40. B. Keimer, N. Belk, R. J. Birgeneau, A. Cassanho, C. Y. Chen, M. Greven, M. A. Kastner, A. Aharony, Y. Endoh, R. W. Erwin, and G. Shirane, Phys. Rev. B **46**, 14034 (1992).
41. V. Barzykin and D. Pines, Phys. Rev. B **52**, 13585 (1995).
42. J. G. Tobin, C. G. Olson, C. Gu, J. Z. Liu, F. R. Solal, M. J. Fluss, R. H. Howell, J. C. O'Brien, H. B. Radousky, and P. A. Sterne, Phys. Rev. B **45**, 5563 (1992).
43. K. Gofron, J. C. Campuzano, H. Ding, C. Gu, R. Liu, B. Dabrowski, B. W. Veal, W. Cramer, and G. Jennings, J. Phys. Chem. Sol. **54**, 1193 (1993).
44. A. A. Abrikosov, J. C. Campuzano, and K. Gofron, Phys. C: Supercond. **214**, 73 (1993).
45. D. S. Dessau, Z.-X. Shen, D. M. King, D. S. Marshall, L. W. Lombardo, P. H. Dickinson, A. G. Loeser, J. DiCarlo, C.-H. Park, A. Kapitulnik, and W. E. Spicer, Phys. Rev. Lett. **71**, 2781 (1993).
46. D. M. King, Z. X. Shen, D. S. Dessau, D. S. Marshall, C. H. Park, W. E. Spicer, J. L. Peng, Z. Y. Li, and R. L. Greene, Phys. Rev. Lett. **73**, 3298 (1994).
47. P. Aebi, J. Osterwalder, P. Schwaller, L. Schlapbach, M. Shimoda, T. Mochiku, and K. Kadowaki, Phys. Rev. Lett. **72**, 2757 (1994).
48. S. V. Borisenko, M. S. Golden, S. Legner, T. Pichler, C. Dürr, M. Knupfer, J. Fink, G. Yang, S. Abell, and H. Berger, Phys. Rev. Lett. **84**, 4453 (2000).
49. V. V. Val'kov, D. M. Dzebisashvili, and A. F. Barabanov, Phys. Lett. A **379**, 421 (2015).
50. V. Val'kov and F. Fedoseev, Theor. Math. Phys. **168**, 1216 (2011).
51. J. M. Tranquada, A. H. Moudden, A. I. Goldman, P. Zolliker, D. E. Cox, G. Shirane, S. K. Sinha, D. Vaknin, D. C. Johnston, M. S. Alvarez, A. J. Jacobson, J. T. Lewandowski, and J. M. Newsam, Phys. Rev. B **38**, 2477 (1988).
52. M. S. Hybertsen, M. Schlüter, and N. E. Christensen, Phys. Rev. B **39**, 9028 (1989).

Translated by K. Kugel